DESIGN, FABRICATION AND TESTING OF FIXED-VALVE MICRO-PUMPS

Fred K. Forster[1] **and Ronald L. Bardell**
Department of Mechanical Engineering

Martin A. Afromowitz and Nigel R. Sharma
Department of Electrical Engineering

Alan Blanchard
Department of Molecular Biotechnology

University of Washington
Seattle, Washington

ABSTRACT

Micro-fluidic systems rely on positive displacement pumps to move fluid due to the low Reynolds numbers encountered at flow rates that are typically in a range around $100\,\mu\mathrm{l/min}$. These pumps are usually reciprocating devices due to limitations of rotating machinery at small scales. Valves for micro-pumps are not necessarily scaled-down macro-valve designs. Existing designs range from passive membranes to complex thermally-controlled active devices. A simpler idea and one that may be more applicable to particulate-laden fluids is a valve that is fixed in shape. Such a valve operates solely by the differential pressure characteristics in each flow direction, which are caused by the flow through it. Such fixed or no-moving-parts (NMP) valves are attractive due to their simplicity of fabrication but have not been studied in enough detail to determine optimal designs. We present design and testing techniques for use in developing efficient NMP valves and for comparing various designs. These techniques were applied to diffuser and valvular conduit designs etched on silicon. Valve performance was characterized by flow resistance and by diodicity, which is the ratio of pressure losses in the reverse to forward direction. Techniques for measuring diodicity in steady and transient flow were developed, and both viscous and dynamic loss contributions to valve performance were analyzed. Computational techniques were used to demonstrate their use in the design of efficient valves.

---

[1]Direct correspondence by e-mail to forster@u.washington.edu

NOMENCLATURE

D_i	Diodicity
f	Circular frequency (Hz)
g	Acceleration of gravity
h	Pressure head (m)
n	Power of velocity to which Δp is proportional
p_c	Pump internal cavity gage pressure
q	Volume flow rate (m^3/s)
Re	Reynolds number
t	Time
v	Flow velocity
$V_c(t)$	Instantaneous pump cavity volume
v_0	Pump cavity volume change
V_0	Nominal pump cavity volume
β	Proportionality constant
Δp	Valve pressure drop
ξ	Pressure loss coefficient
ρ	Mass density (kg/m^3)

INTRODUCTION

Numerous micro-pump designs have been developed over the last few years (Schomburg et al., 1993; Shoji and Esashi, 1994). Positive displacement pumps are the most common type due to the low Reynolds number at which micro-fluidic devices typically operate. Almost all positive displacement micro-pumps are of the reciprocating type, and require valves. Such pumps usually consist of a simple cavity that can be varied in volume in a periodic manner by deforming a plate covering the

cavity, and inlet and outlet valves that allow more flow through the outlet than the inlet under positive cavity pressure.

Due to the inherent difficulty of down-sizing macro-scale valve technology, micro-valves represent a significant challenge in the design of miniature pumping systems. Valves that have no moving parts may have distinct advantages over macro-scale designs. Moreover, micro-pumps designed to move fluid containing particulates or cellular material whose size may be on the same order as that of the flow channels may require valves with no moving parts. Applications where such situations are expected are in biotechnology, environmental testing and instrumentation for analytical chemistry.

The performance of a NMP valve can be represented by a number of parameters, the most important of which is the ratio of pressure drop in the reverse flow direction to that in the forward direction at the same flow rate. This ratio is denoted by diodicity

$$D_i = \Delta p_r / \Delta p_f, \qquad (1)$$

where r and f refer to reverse and forward flow directions, respectively. Diodicity is, in general, a function of flow rate. It is also a quantitative measure of flow delivery efficiency, which can be seen if a pump is considered going through its outflow stroke with both input and output valves exposed to atmospheric pressure so that $p_c = \Delta p_f = \Delta p_r$. Next consider the volume flow rate out the inlet valve given by q, and that out the outlet given by $q + \Delta q$. Note that with NMP valves there may be significant flow out of both inlet and outlet. If the pressure flow relation for each valve is given by $\Delta p_f = \beta_f v_f^n$ and $\Delta p_r = \beta_r v_r^n$, the flow delivery efficiency can be expressed as

$$\frac{\Delta q}{q} = \frac{D_i - 1}{n}. \qquad (2)$$

Above, β is a proportionality constant. The case of $n = 2$ represents dynamic losses through the valves where $\beta = \xi \frac{1}{2}\rho$, and where ξ is the pressure loss coefficient. The case of $n = 1$ represents pure viscous losses.

The first NMP valve reported in the literature for micro-pumps utilizes a pair of diffusers, i.e. a converging/diverging nozzle (Stemme and Stemme, 1993). A pump design utilizing these diffuser valves operates in a range of approximately 2,000 to 20,000 μl/min and utilizes machined brass valves. While these flow rates are two to three orders of magnitude higher than desired, the work demonstrates the application of high Reynolds number diffuser data to design diffusers operating at relatively low Reynolds numbers.

In designing the valves described above, the authors assumed that pressure losses in the valve were dynamic losses, i.e. proportional to velocity squared. However, as the size scale decreases, the possibility of losses primarily due to viscous effects proportional to velocity increases. The impact of this assumption on design can be seen by considering harmonic pumping with the instantaneous pump cavity volume given by

$$V_c(t) = V_0 + v_0 \sin 2\pi f t. \qquad (3)$$

The relationship between the net volume flow rate of the pump q_{net} and D_i can be derived for an incompressible fluid by considering conservation of mass and an assumed relation between pressure loss and flow. The result is given by the relations

$$\frac{q_{\text{net}}}{2fv_0} = \frac{D_i^{1/n} - 1}{D_i^{1/n} + 1}, \quad D_i > 1, \qquad (4)$$

or

$$D_i = \left(\frac{1 + q_{\text{net}}/2v_0 f}{1 - q_{\text{net}}/2v_0 f} \right)^n, \quad q_{\text{net}} < 2v_0 f, \qquad (5)$$

where the viscous and dynamic cases correspond to $n = 1, 2$, respectively. The results for $n = 2$ agree with Stemmes' results with the diodicity being the ratio of pressure loss coefficients $D_i = \xi_r/\xi_f$. In either case, q_{net} monotonically increases as D_i increases, and approaches $2fv_0$ asymptotically as shown in Fig. 1. More importantly Fig. 1 shows that for dynamic losses the diodicity must be significantly higher for the same net flow compared to the case of viscous losses. This represents one possible advantage at small scales where at low Reynolds number viscous losses may dominate dynamic losses.

There are two problems with Eqs. 4 and 5. First, the effect of n shown in Eq. 4 prevents that equation from being accurate for design because for $D_i \simeq 1$ an estimate of q_{net} with $n = 1$ is 100% higher than that calculated with $n = 2$. In addition, Eq. 5 cannot be used to estimate diodicity unless n is known.

The shortcomings of the above relations can be circumvented by considering a simple experimental setup that can be used to determine diodicity nonparametrically, i.e. without utilizing information on the character of the valve losses. At block load pressure, i.e. when $q_{\text{net}} = 0$, the pump oscillates in a symmetrical breathing mode with the same amount of fluid moving in and out the inlet and outlet valves. The equality of these flow rates expressed in terms of pressure drops yields an equation identical to Eq. 1 regardless of whether pressure loss is proportional to velocity or velocity squared. If the inlet and outlet pressure heads are h_i and h_o, respectively, $\Delta p_f = p_c - \rho g h_o$, and $\Delta p_r = p_c - \rho g h_i$. The
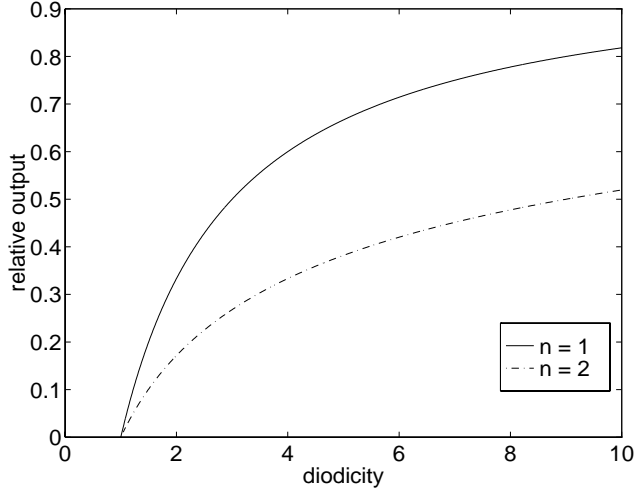
FIGURE 1: RELATIVE NET VOLUME FLOW RATE VERSUS DIODICITY FROM EQ. 4.

FIGURE 2: DIFFUSER VALVE (D01-R).

time average of the resulting equation yields

$$D_i = \frac{1 - \rho g h_i / \overline{p_c}}{1 - \rho g h_o / \overline{p_c}}. \qquad (6)$$

With $\rho g h_i$, $\rho g h_o$ and $\overline{p_c}$ known, the operational (as compared to steady-state) determination of D_i can be made. Comparisons of estimates for D_i from the above equation, from Eq. 5 and from steady-flow experiments can be used to investigate dynamic effects during actual pump operation.

We present methods and results that demonstrate our test and design procedures for NMP valves based concepts described above.

METHODS
Fabrication

Pump chambers with valves were etched on silicon wafers. Two types of valves were fabricated. The first type was a diffuser valve (D01-R) shown in Fig. 2. This valve was etched using reactive ion etching (RIE). The geometry of the valve was obtained from performance maps for macroscopic planar diffusers, which are based on significantly higher Reynolds numbers due to the lack of data at low Reynolds number (White, 1994; Bardina et al., 1981). The diffuser throat width was $142\,\mu$m. The length and width of the forward flow diffuser section was 1300 and $442\,\mu$m, respectively. The length and width of the reverse flow diffuser section was 350 and $642\,\mu$m, respectively. The depth of the etching was $60\,\mu$m.

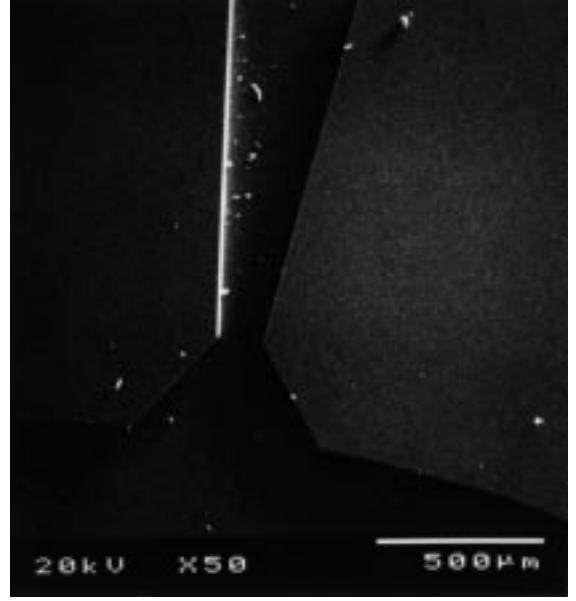The valve shown in Fig. 3 is a valvular conduit (T45-R) that has not been used previously for micro-flow

applications (Tesla, 1920). As with valve D01-R, valve T45-R was etched using RIE. The conduit width was $114\,\mu$m. It was etched to the same depth as D01-R.

A third pump (D01-A, not shown) was fabricated from the same mask pattern as D01-R but etched using standard anisotropic (EDP) wet etching to a depth of $30\,\mu$m, one half the depth of the RIE devices. Due to the etching process the walls of the pump cavity and valves were sloped such that their lateral dimensions decreased with depth whereas RIE produced essentially vertical walls. The slope of the wall varied with local orientation relative to the silicon crystal plane, but was typically $50\,^\circ$ from vertical.

Individual pump chips were diced from the etched wafers. The pump cavities were $10\,$mm in diameter. The floor of each pump cavity was drilled to provide a central $700\,\mu$m diameter port for pressure measurements. Pyrex pump cover plates were $150\,\mu$m thick, drilled for inlet and outlet ports, and anodically bonded to the silicon chips.

The driving element for each pump consisted of a $5\,$mm diameter piezoelectric disk fabricated from $190\,\mu$m thick PZT sheet stock (Piezo Systems, Inc., Cambridge MA). The disk was centered over the pump chamber and bonded to the outer side of the cover plate using silver conductive epoxy, which was also used to attach electrical leads.
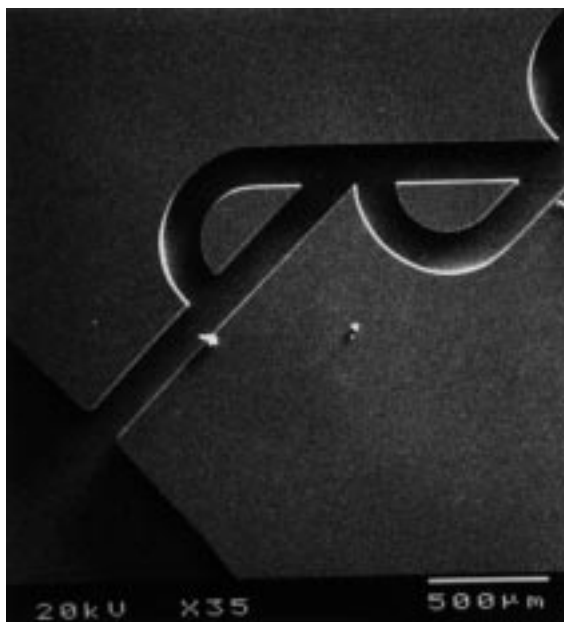
FIGURE 3: VALVULAR CONDUIT (T45-R).

Computational Fluid Dynamics

Individual valves were modelled with a finite-element code (FLOTRAN, Compuflo, Inc., Houston, PA). Both 2-D and 3-D models were developed, but the 2-D models were used to obtain initial results. Steady flow models were used to evaluate relative pressure drops across valves at various flow rates, and to identify flow-loss mechanisms from calculated velocity field patterns. The models were meshed with tetrahedral elements using higher grid densities near walls and other regions with high velocity gradients. Relaxation was employed to enhance convergence, but no dissipative damping techniques were employed. The calculations were allowed to proceed until the residual fields reached acceptably low levels.

Bench Testing

Completed silicon pump chips were attached to a steel jig. The jig consisted of a backing plate that held a pressure transducer in a sealed cavity behind the pump cavity pressure tap. The jig also incorporated inlet and outlet tubing brackets that held two 18-gauge blunt tip needles sealed with O-rings.

All bench tests were performed with room temperature water that was degassed by heating. For steady-state tests the pressure drop across an entire pump (across both valves) was measured with a mercury manometer while flow was forced through the pump

with a gear-driven infusion pump. Volume flow rate was measured by collecting fluid over a known time, essentially a micro-bucket and stopwatch technique.

Pump performance was characterized by measuring the fluid levels in identical vertical Teflon tubes 0.9 mm in diameter attached to the inlet and outlet ports of the pump. The diameter of the Teflon tubes was chosen to eliminate dynamic effects of fluid in the tubes. Pump activation was initiated with the fluid levels equalized. An exponential curve fitted to the height of the outlet column as a function of time was differentiated to estimate net volume flow.

Instantaneous pump cavity pressure and instantaneous pump cover plate transverse velocity were measured during pump operation. The pressure was measured with a 1.3 mm diameter strain gage pressure transducer (Entran, Model EPI-127, Fairfield, NJ). Velocity was measured with a laser vibrometer (Polytec, Model OVF 302, Waldbronn Germany). The pump-holding fixture described above was mounted in a computer-controlled traversing stage to allow for velocity measurements across the entire cover plate surface. The excitation voltage, pressure and velocity signals were digitized simultaneously at a sampling frequency of 20 kHz for each signal (Model AT-MIO-16E-2 A/D module and Labview v3.1.1 data acquisition software, National Instruments Austin, TX), and stored on magnetic disk on a PC. Displacements were calculated by integrating the velocity signal.
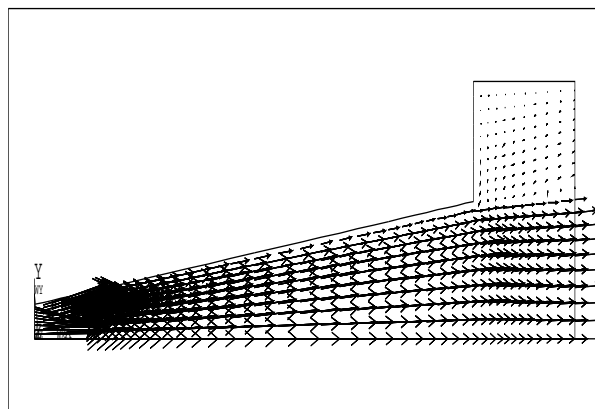

FIGURE 4: CALCULATED VELOCITY-FIELD IN THE FORWARD DIFFUSER SECTION OF VALVE DURING FORWARD FLOW. FLOW RATE 60 μL/MIN (THROAT RE = 10).

RESULTS AND DISCUSSION

The numerically-calculated forward- and reverse-flow velocity fields are shown for the D01-R diffuser valve in

Figs. 4 and 5. The arrows represent the direction and magnitude of local velocity. The forward flow case in Fig. 4 shows the velocity profile developing near the wall as the flow moves downstream, but separation does not occur until the sudden expansion is reached at the end of the diffuser. In contrast, Fig. 5 shows separation occurring immediately after the throat, forming a jet with entrainment and recirculation. The calculated behavior was consistent with desired design goals.
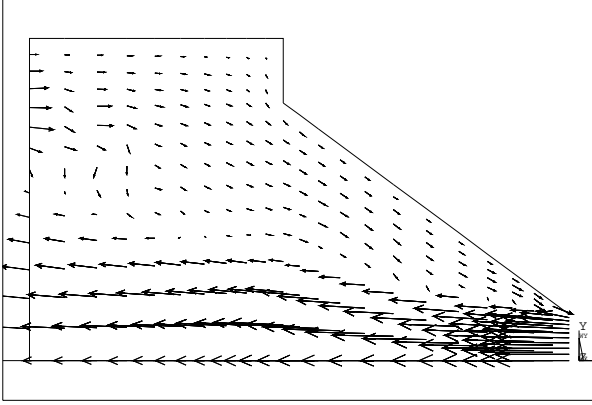

FIGURE 5: CALCULATED VELOCITY-FIELD IN THE REVERSE DIFFUSER SECTION OF VALVE DURING REVERSE FLOW. FLOW RATE 42 μL/MIN (THROAT RE = 6).

direction	fit	D01-R	T45-R	D01-A
reverse	linear	0.022*	0.025	0.004*
	quadratic	0.024	0.020*	0.050
forward	linear	0.020*	0.017*	0.006*
	quadratic	0.028	0.029	0.050

TABLE 1: STANDARD ERROR OF LINEAR AND QUADRATIC CURVES. AN ASTERISK DENOTES THE FITTING FUNCTION CHOSEN.

The steady-flow valve pressure loss characteristics are shown in Fig. 6. Linear and quadratic curves were fit to the data. The standard error of the y-estimate was used as a quantitative indication of how well the behavior could be modeled by simple viscous or simple dynamic effects. The results are shown in Table 1. These preliminary results indicate measurable differences in behavior. Valve D01-R does not appear to have losses distinctly characterized as viscous or dynamic. In the case of valve D01-A viscous losses appear to dominate. Valve D01-A is one half the depth of valve D01-R and thus the Reynolds number is apparently governed by the reduced depth of this valve. Valve T45-R demonstrated viscous behavior in the forward direction and dynamic behavior
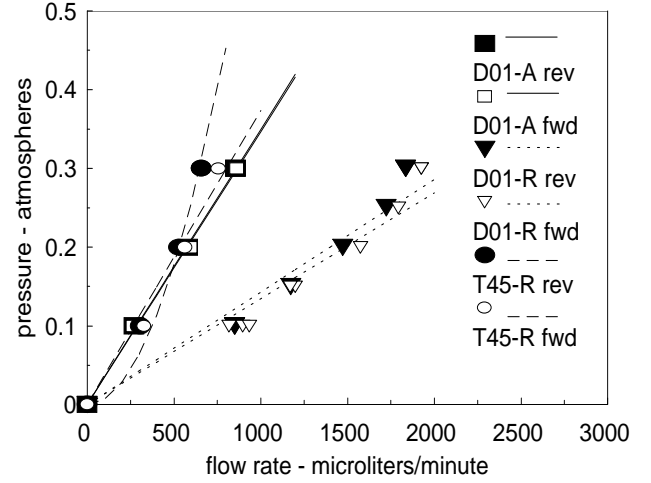

FIGURE 6: PRESSURE LOSS CHARACTERISTICS PER VALVE.

in the reverse direction. The dynamic behavior during reverse flow may be due to momentum interactions at channel bifurcations.

A steady-flow diodicity curve was determined for each valve according to Eq. 1 using the regression curves chosen above The resulting curves are shown in Fig. 7, which also shows discrete diodicity estimates calculated directly from the data. From its definition diodicity is independent of flow rate when losses are either linear or quadratic in both directions. Both diffuser valves display this behavior. Valve T45-R exhibits a diodicity that increases rapidly with flow rate due to the apparent difference in loss mechanisms in the two flow directions.
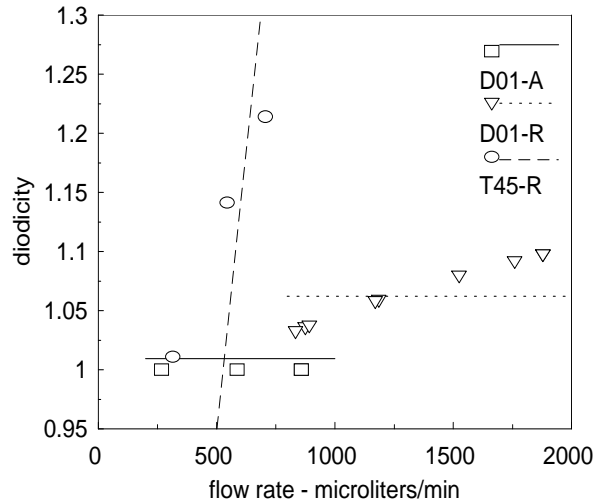

FIGURE 7: STEADY-FLOW DIODICITY.

Figs. 6 and 7 indicate that trade-offs may be required to optimize valve performance. Ideally a well-designed NMP valve will have both high diodicity and low flow resistance. These characteristics along with other factors including fluid inertance can be studied more thoroughly with instantaneous measurements of basic pump variables, particularly pressure and volume displacement. The average internal pressure is a direct measure of diodicity (Eq. 6), and peak negative pressure is correlated with pumping limitations due to cavitation.
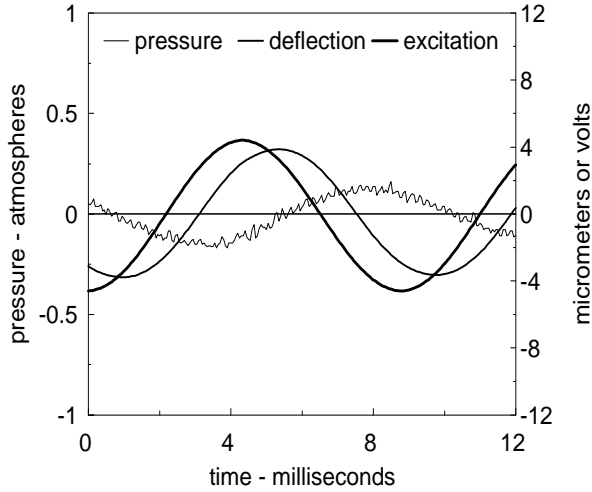

FIGURE 8: INSTANTANEOUS PRESSURE AND DEFLECTION FOR HARMONIC EXCITATION OF 150 V.
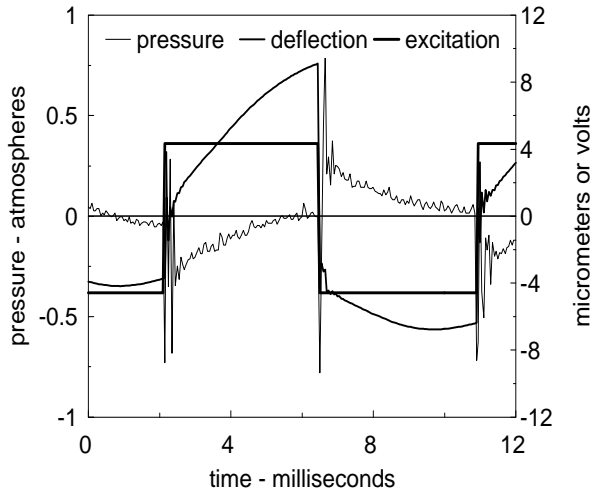

FIGURE 9: INSTANTANEOUS PRESSURE AND DEFLECTION FOR SQUARE-WAVE EXCITATION OF 150 V.

Typical recordings of instantaneous pump signals are shown in Figs. 8 and 9. Shown are harmonic and square wave excitations applied to the driver amplifier, the unfiltered cavity pressure and the cover plate outward deflection at its center. The pump with D01-R valves was used to generate these data. A driving frequency of 114 Hz was used, which was the frequency for maximum net flow rate at zero pump head. The peak excitation voltage was the same in both cases, but the pump output was significantly larger for the square wave excitation, 38 µl/min versus 5.5 µl/min. This output ratio of over six indicates the importance of waveform shape. Also of note is the asymmetry of the membrane deflection and the large pressure spikes during excitation.

CONCLUSIONS

Design and testing techniques were applied to micropumps with valves having no moving parts. Diffuser and valvular conduit designs were studied. The valvular conduit was found to have higher volumetric efficiency (diodicity) possibly due to dynamic pressure losses in one flow direction and viscous losses in the other. Dynamic measurements of pump driving element displacement and pump internal pressure showed important details of pump operation.

ACKNOWLEDGEMENTS

REFERENCES

Bardina, J., Lyrio, A., Kline, S. J., Ferziger, J. H., and Johnston, J. P. (1981). A prediction method for planar diffuser flows. *Trans. ASME J. Fluids Eng.*, 103:315–321.

Schomburg, W. K., Fahrenberg, J., Maas, D., and Rapp, R. (1993). Active valves and pumps for microfluidics. *J. Micromech. Microeng.*, 3:216–218.

Shoji, S. and Esashi, M. (1994). Microflow devices and systems. *J. Micromech. Microeng.*, 4:157–171.

Stemme, E. and Stemme, G. (1993). A valveless diffuser/nozzle-based fluid pump. *Sens. and Actuators A*, 39:159–167.

Tesla, N. (1920). Valvular conduit. *U.S. Patent No. 1,329,559.*

White, F. M. (1994). *Fluid Mechanics, 3rd Ed.* McGraw-Hill, Inc., New York.